

Optimizing neutron moderators for a spallation-driven ultracold-neutron source at TRIUMF

W. Schreyer^a, C. A. Davis^a, S. Kawasaki^b, T. Kikawa^c, C. Marshall^a, K. Mishima^d, T. Okamura^b, R. Picker^{a,e}

^aTRIUMF, Vancouver, BC V6T 2A3, Canada

^bKEK, Tsukuba 305-0801, Japan

^cKyoto University, Kyoto 606-8501, Japan

^dJ-PARC, Tokai 319-1195, Japan

^eSimon Fraser University, Burnaby, BC V5A 1S6, Canada

Abstract

We report on our efforts to optimize the geometry of neutron moderators and converters for the TRIUMF UltraCold Advanced Neutron (TUCAN) source using MCNP simulations. It will use an existing spallation neutron source driven by a 19.3 kW proton beam delivered by TRIUMF's 520 MeV cyclotron. Spallation neutrons will be moderated in heavy water at room temperature and in liquid deuterium at 20 K, and then superthermally converted to ultracold neutrons in superfluid, isotopically purified ⁴He. The helium will be cooled by a ³He fridge through a ³He-⁴He heat exchanger.

The optimization took into account a range of engineering and safety requirements and guided the detailed design of the source. The predicted ultracold-neutron density delivered to a typical experiment is maximized for a production volume of 27 L, achieving a production rate of $1.4 \cdot 10^7 \text{ s}^{-1}$ to $1.6 \cdot 10^7 \text{ s}^{-1}$ with a heat load of 8.1 W. At that heat load, the fridge can cool the superfluid helium to 1.1 K, resulting in a storage lifetime for ultracold neutrons in the source of about 30 s. The most critical performance parameters are the choice of cold moderator and the volume, thickness, and material of the vessel containing the superfluid helium.

The source is scheduled to be installed in 2021 and will enable the TUCAN collaboration to measure the electric dipole moment of the neutron with a sensitivity of 10^{-27} e cm .

Keywords: Ultracold neutrons, moderator, spallation, superfluid helium

1. Introduction

If neutrons are slowed below a certain energy, their wavelengths become long enough that they cannot resolve the strong potential of individual nuclei anymore. Instead, materials appear as a constant average potential that can reach several hundred nanoelectronvolts. [1] predicted that neutrons with energies below that potential would be totally reflected from such surfaces and could be trapped for long periods of time, making these “ultracold” neutrons (UCN) an ideal tool to measure the properties of neutrons with high precision. This phenomenon was first experimentally confirmed by [2, 3].

These early experiments separated ultracold neutrons from the low-energy tail of a thermal neutron spectrum produced in reactors with graphite, water, or polyethylene moderators [2, 4, 5]. Ultracold neutrons were reflected along a curved tube while neutrons with higher energies can penetrate it and are absorbed in the surrounding material. The first dedicated sources made use of a larger portion of a thermal neutron spectrum by extracting neutrons vertically from a cold moderator [3, 6],

reducing their kinetic energy by the gravitational potential of 102.5 neV m^{-1} , and eventually reflected them off moving blades mounted on a “turbine” [7, 8] to slow them to ultracold velocities.

The density of ultracold neutrons that these sources can provide is limited by Liouville's theorem. To overcome this limitation, [9, 10] suggested a “superthermal” source. In suitable materials called converters, e.g. superfluid ⁴He or solid deuterium, neutrons can induce solid-state excitations and lose virtually all their energy and momentum. The inverse process of upscattering can be suppressed if the material is cooled to low enough temperatures. ⁴He does not absorb neutrons at all, making it possible to increase the lifetime of ultracold neutrons to hundreds of seconds if cooled below 1 K.

Despite this obvious advantage of superfluid ⁴He, the first superthermal sources in operation were based on solid deuterium [11, 12, 13]. Although absorption and upscattering of ultracold neutrons in solid deuterium limits the UCN lifetime to less than 150 ms, solid deuterium has a higher UCN-production cross section and can convert a wider range of neutron energies to UCN. Hence, if the solid deuterium is coupled to a large storage volume, the ultracold neutrons are quickly separated from the converter and

Email address: wschreyer@triumf.ca (W. Schreyer)

can be stored for longer times. Such a source can reach a performance similar to a superfluid-helium source, while operating at a more manageable temperature of about 5 K. These sources rely on cold polyethylene [11], heavy water and solid hydrogen [12], or heavy water and the solid deuterium itself [13] as moderators. Two more reactor sources using solid deuterium are currently in construction, using solid-hydrogen [14] and solid-methane moderators [15].

To achieve the low temperatures required for a superfluid-helium converter, the first attempts at KEK [16] converted a cold-neutron beam to ultracold neutrons to reduce the heat load and therefore required no moderators. This concept is now in operation for a source at Institut Laue-Langevin [17] but can also be used to produce ultracold neutrons directly in an experiment cell [18, 19]. These sources are limited by the lower intensities of collimated neutron beams, but concepts that could reach production rates similar to the planned source at TRIUMF at significantly lower heat loads have been proposed [20].

[21] demonstrated that with a ^3He fridge it is possible to reach the low temperature required for a superfluid-helium source close to a neutron spallation target. This source was later moved to a new spallation target with up to 50 times more beam power (40 μA , 483 MeV, 19.3 kW) at TRIUMF [22, 23]. Thanks to a fast kicker magnet [24], this spallation target can be irradiated for arbitrary durations, allowing to optimally match the irradiation time to experimental requirements and reducing the heat load whenever no UCN production is required. This feature provides a major advantage over reactor sources, which have to continuously operate at full cooling power, and other spallation sources, which are irradiated with short beam pulses at fixed intervals.

The source at TRIUMF will undergo an upgrade in 2021 to make use of the full beam power available and enable a measurement of the electric dipole moment of the neutron with a sensitivity of $10^{-27} e \text{ cm}$. The main limitation to scaling up the beam power is the increasing heat load that has to be removed from the very cold converter. Hence, projects aiming for even higher UCN production in superfluid helium generally plan to operate at higher temperatures [25, 26], at the cost of increased losses that partially negate the gains in UCN production.

This publication describes how we optimized the neutron moderators and converter for the upgraded TRIUMF UltraCold Advanced Neutron (TUCAN) source, taking into account detailed engineering requirements like pressure-vessel thicknesses, safety restrictions, material activation, and biological shielding.

2. A superfluid ^4He converter

^4He in its superfluid state He-II can convert cold neutrons with an energy of 1 meV to ultracold neutrons through single-phonon excitation and, to a smaller degree, through multi-phonon excitation at slightly higher energies [27, 28],

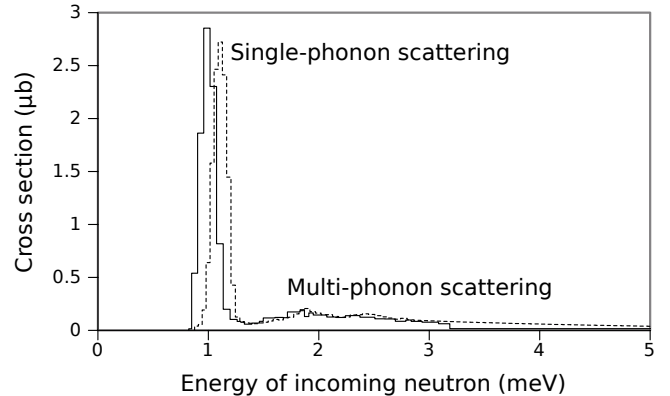


Figure 1: Cross sections for production of ultracold neutrons with energies up to 233.5 meV in superfluid ^4He , calculated from [27] (solid line) and [28] (dashed line).

see Fig. 1. To maximize the UCN production, the neutron flux at 1 meV should be maximized by moderating it to an effective neutron temperature of 7.7 K. Cold-neutron sources providing neutrons at these temperatures often use a two-stage moderation first in water and then liquid hydrogen. While hydrogen has a large neutron-scattering cross section, leading to very rapid moderation that is useful for pulsed sources, deuterium has a much smaller neutron-absorption cross section. Hence, heavy water and liquid deuterium are often preferable for continuous sources.

The total loss rate τ^{-1} of UCN in a volume filled with superfluid helium is given by the sum of all loss channels

$$\tau^{-1} = \tau_{\text{He}}^{-1} + \tau_{\text{abs}}^{-1} + \tau_{\text{wall}}^{-1} + \tau_{\beta}^{-1}. \quad (1)$$

The upscattering loss rate of UCN in superfluid ^4He , τ_{He}^{-1} , is strongly temperature dependent and scales with

$$\tau_{\text{He}}^{-1} = B \left(\frac{T}{1 \text{ K}} \right)^7, \quad (2)$$

with an upscattering parameter B between 0.008 s^{-1} and 0.016 s^{-1} [9, 29, 22]. The other stable helium isotope, ^3He , has an extremely large neutron-absorption cross section. In natural helium with a ^3He abundance of 10^{-6} to 10^{-7} the absorption lifetime τ_{abs} is less than 100 ms. To reduce the upscattering and absorption losses to a similar level as the losses at the walls $\tau_{\text{wall}}^{-1} \lesssim (100 \text{ s})^{-1}$, the superfluid helium has to be isotopically purified to reduce the ^3He abundance to below 10^{-10} and cooled to temperatures of 1 K or less.

With these improvements, the storage lifetime of ultracold neutrons in a source filled with superfluid helium can reach hundreds of seconds. Once UCN production with production rate P is started, ultracold neutrons will accumulate in the source and their density ρ in a volume V

$$\rho = \frac{P\tau}{V} \left(1 - e^{-t/\tau} \right) \quad (3)$$

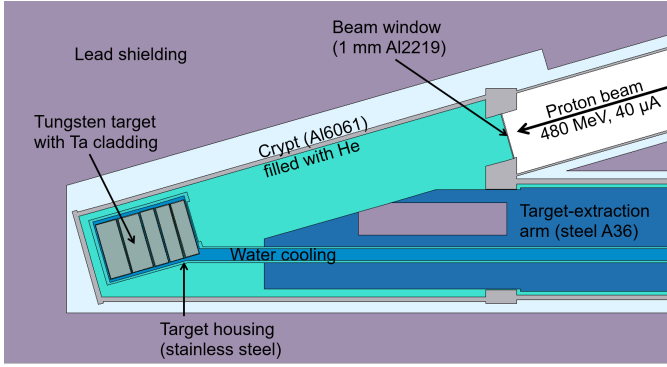


Figure 2: MCNP model of the neutron spallation target (top view)

will reach an equilibrium value $P\tau/V$ after a production time t much longer than the storage lifetime τ .

The ultimate limit is given by the beta-decay lifetime of free neutrons $\tau_\beta = (879.4 \pm 0.6) \text{ s}$ [30].

3. Simulation model

To estimate and optimize the performance of the upgraded ultracold-neutron source at TRIUMF, we built a detailed model to simulate it with MCNP 6.1 [31]. The $40 \mu\text{A}$ beam of 483 MeV protons from TRIUMF's cyclotron hits the neutron spallation target, see Fig. 2, and produces secondary protons, neutrons, electrons, and gamma photons. MCNP simulates the interaction of those particles with surrounding materials with detailed and well-benchmarked scattering models [32]. Many of the materials used in the simulation had realistic compositions determined from assays, see table 1. For the other materials, typical compositions were used with the conservative assumption that all impurities are at their maximum allowed levels with natural isotopic abundances.

We benchmarked this simulation model against the prototype source currently in operation at TRIUMF and achieved a good match between the simulated and measured UCN yield [22]. However, large uncertainties in the simulations of UCN storage and transport could potentially mask under- or over-estimations in UCN production of as much as 30 %.

3.1. UCN production and heat load

We determined UCN production P from an MCNP flux tally, multiplying the neutron flux in the UCN converter Φ with the UCN-production cross section σ taken from [27, 28], see Fig. 1:

$$P = \int \Phi(E)\sigma(E)dE. \quad (4)$$

MCNP also provides the average heat deposited per primary proton in each part of the model. Typically, there

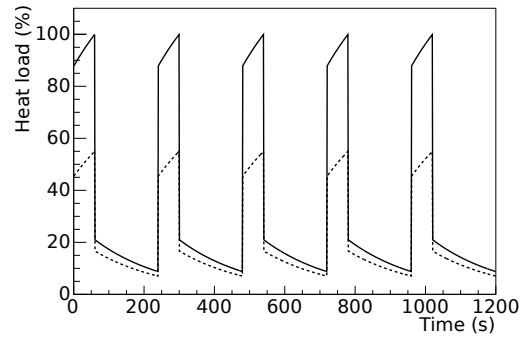


Figure 3: Time structure of heat load (solid line) on the converter and its aluminium vessel during irradiation with a duty cycle of 25 % (beam on for one minute, beam off for three minutes). The dashed line is the fraction deposited in the vessel wall. Static heat load is not included.

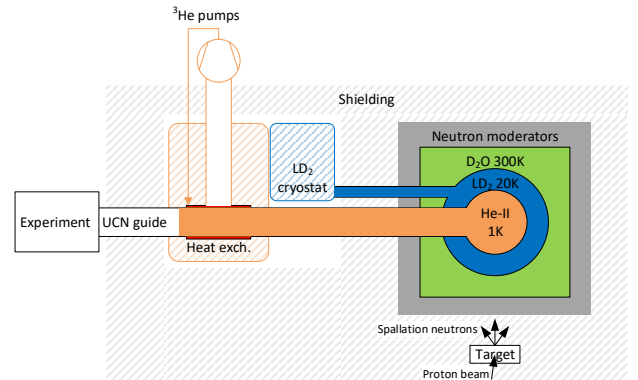


Figure 4: Conceptual sketch of the upgraded UCN source at TRIUMF. The proton beam points into the page.

is a large prompt heat deposited followed by a slowly decaying heat load caused by radioactive decays. To calculate the total heat load during or after a continuous irradiation, this heat-load profile is convolved with the intensity and duty cycle of the irradiation. For these simulations we assumed a duty cycle for a typical UCN experiment that is filled for one minute while the target is irradiated with $40 \mu\text{A}$, and then stops the irradiation while UCN are stored and detected for three minutes, corresponding to a duty cycle of 25 %, see Fig. 3.

The heat load calculated in MCNP does not include any static heat load on the cryogenic parts due to thermal conduction, convection, or radiation. For the estimation of the converter temperature we added a static heat load between 0 W and 1 W.

3.2. UCN-converter temperature and storage lifetime

The converter will be cooled by a ^3He fridge. A copper heat exchanger filled with about 300 mL of liquid ^3He is cooled to 0.8 K to 0.9 K by lowering the vapor pressure with an array of vacuum pumps with a pumping speed S of up to $10\,000 \text{ m}^3 \text{ h}^{-1}$. To shield the fridge from the

Table 1: Material compositions used in the simulation model. Compositions of stainless steel, lead, graphite, and steel shielding were assayed by mass and optical spectrometry [33, 34].

Material	Density (g/cm ³)	Composition (weight-%)
Air	0.00120	75.2 N, 23.2 O, 1.28 Ar, 0.0125 C
Al6061	2.70	95.85 Al, 1.2 Mg, 0.8 Si, 0.7 Fe, 0.4 Cu, 0.35 Cr, 0.25 Zn, 0.15 Mn, 0.15 Ti
Al2219	2.84	91.5 Al, 6.8 Cu, 0.4 Mn, 0.3 Fe, 0.2 Si, 0.15 V, 0.15 Zr, 0.1 Ti, 0.1 Zn, 0.02 Mg
AlBeCast 910 [35]	2.17	57 Be, 38 Al, 3.4 Ni, 0.5 Si, 0.3 Fe, 0.24 O
AlBeMet 162 [36]	2.10	62 Be, 38 Al
Beryllium	1.85	100 Be
Bismuth	9.75	100 Bi
Copper	8.96	100 Cu
Graphite	1.70	99.978 C, 0.0125 V, 0.0033 Ti, 0.0026 Fe, 0.0014 Al, 0.0006 Ca, 0.0004 Ni, 0.0003 B, 0.0002 K, 0.0002 Si, 0.00016 Zr, 0.0001 Cu, 0.0001 Pb, 0.00006 Zn, 0.00005 Na, 0.00003 Cr, 0.00003 Co, 0.00002 Mg, 0.00002 Mn, 0.00002 Gd, 0.000003 Li
Aluminium	2.70	100 Al
AZ 80	1.80	90.85 Mg, 8.5 Al, 0.5 Zn, 0.15 Mn
Beralcast 310 [37]	2.16	60 Be, 36 Al, 2.5 Ag, 0.25 Si, 0.2 Co, 0.2 Ge, 0.2 Fe
Heavy water	1.10	100 ² H ₂ O
He gas	0.000180	100 He
Lead	11.4	99.9915 Pb, 0.004 Bi, 0.001 Cu, 0.0008 Ag, 0.0008 Sb, 0.0005 As, 0.0005 Sn, 0.0005 Fe, 0.0004 Zn
LD ₂	0.160	100 ² H ₂
Liquid ³ He	0.082	100 ³ He
Magnox AL80	1.80	99.2 Mg, 0.8 Al, 0.004 Be
Mild steel	7.80	98 Fe, 1 Mn, 0.4 C, 0.28 Si, 0.2 Cu, 0.05 S, 0.04 P
Stainless steel	8.00	71.4 Fe, 18 Cr, 8 Ni, 1.32 Mn, 1 Si, 0.095 Co, 0.08 C, 0.045 P, 0.03 S, 0.0075 Nb, 0.0022 As, 0.00036 Sb
Steel shielding	7.36	89.15 Fe, 4.5 Cr, 3.3 Ni, 0.99 Cu, 0.8 Mn, 0.35 Si, 0.32 C, 0.25 Al, 0.16 Mo, 0.015 P, 0.057 Co, 0.027 Pb, 0.021 V, 0.02 S, 0.018 Nb, 0.012 Sn, 0.011 Ti, 0.0011 B
Superfluid He	0.145	100 ⁴ He
Tantalum	16.7	100 Ta
Tungsten	19.3	100 W

high radiation above the target, a 2.5 m-long and 150 mm-diameter conduction channel filled with isotopically purified superfluid ⁴He and surrounded by steel shielding connects the heat exchanger to the UCN converter, see Fig. 4.

To determine the temperature of the superfluid helium we modeled the cooling power of this fridge. The pumps with inlet temperature T_{pump} remove heat

$$Q = \eta_{\text{JT}} \frac{(p(T_{3\text{He}}) - \Delta p) LS}{RT_{\text{pump}}} \quad (5)$$

from the ³He bath with vapor pressure $p(T_{3\text{He}})$, latent heat L , and universal gas constant R . η_{JT} is the fraction of supplied ³He that is converted to liquid during Joule-Thompson expansion and Δp the pressure drop in the pumping duct. The same amount of heat has to be transported across the heat exchanger. This heat transport is limited by the Kapitza resistance at the interface areas $A_{4\text{He}}$ (between liquid ⁴He with temperature $T_{4\text{He}}$ and the copper heat exchanger with temperature T_{Cu}) given by the Acoustic Mismatch Theory [38]:

$$Q = 20 \text{ W m}^{-2} \text{ K}^{-4} \cdot k_G T_{\text{Cu}}^3 |T_{\text{Cu}} - T_{4\text{He}}| A_{4\text{He}}. \quad (6)$$

The Kapitza resistance at the interface area $A_{3\text{He}}$ between heat exchanger and ³He with temperature $T_{3\text{He}}$ is assumed to be 1.2 to 2.6 times higher due to its higher sound velocity:

$$Q = (7.7 \sim 17) \text{ W m}^{-2} \text{ K}^{-4} \cdot k_G T_{\text{Cu}}^3 |T_{\text{Cu}} - T_{3\text{He}}| A_{3\text{He}}. \quad (7)$$

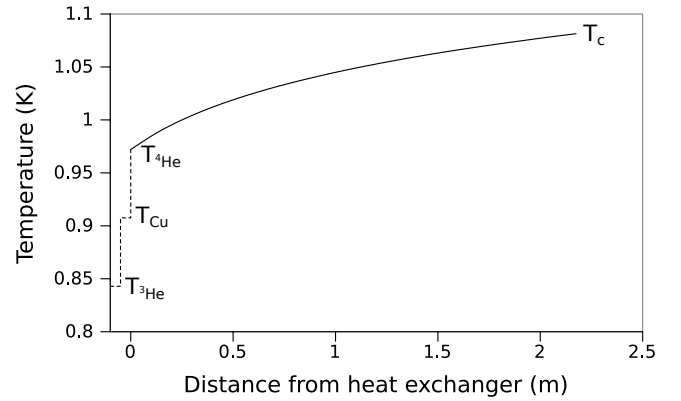


Figure 5: Temperature profile in the conduction channel (solid line) and across the heat exchanger (dashed line). This example assumes $\eta_{\text{JT}} = 0.92$, $\Delta p = 300 \text{ Pa}$, $S = 10\,000 \text{ m}^3 \text{ h}^{-1}$, $T_{\text{pump}} = 300 \text{ K}$, $k_G = 40$, $A_{3\text{He}} = 0.76 \text{ m}^2$, $A_{4\text{He}} = 0.24 \text{ m}^2$, $Q = 8.1 \text{ W} + 1 \text{ W}_{\text{static}}$, and $f(T)^{-1}$ is taken from [39].

The scaling factor k_G is determined by the surface quality of the heat exchanger and typically lies between 20 and 40 [38]. We assume it to be the same for ³He. The heat conduction through the copper itself is large enough to be negligible.

The same amount of heat has to again be transported from the converter volume to the heat exchanger through the channel filled with superfluid helium. The heat trans-

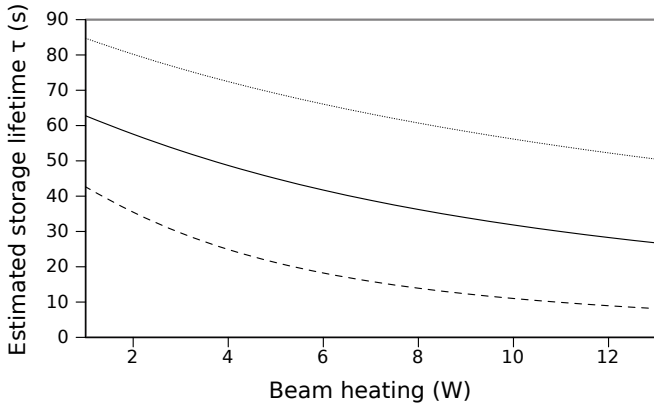


Figure 6: Estimated relations between heat load Q and storage lifetime in the source τ with the most optimistic (dotted line), most pessimistic (dashed line), and an intermediate parameter set (solid line).

ported through a channel with length l and cross section A can be determined with the Gorter-Mellink equation [40]

$$Q = \left(\frac{A^3}{l} \int_{T_{\text{He}}}^{T_c} f(T)^{-1} dT \right)^{1/3}, \quad (8)$$

with an empirical heat-transport function $f(T)^{-1}$ [38, 39]. Fig. 5 shows an example of the resulting temperature profile along the conduction channel and across the heat exchanger.

Solving these equations for the converter temperature T_c gives a relation between Q and T_c that can be approximated with a power law. Combining it with equation (2) yields an upscattering lifetime of

$$\tau_{\text{He}} = B \left(\frac{Q}{1 \text{ W}} \right)^a \quad (9)$$

with B from 500 s to 1500 s and a from -1.5 to -1.0 , see Fig. 6. The heat load Q can also include some static heat load Q_{static} due to thermal radiation, convection, and conduction in the cryostat, which we conservatively assumed can be as large as 1 W.

The converter vessel, conduction channel, and heat exchanger will most likely be coated with NiP. In the NiP-coated prototype source, [21] achieved a total storage lifetime τ of 81 s; our own measurements with a NiP-coated bottle at room temperature with a volume of 6.5 L and a volume-to-surface ratio of 3.37 cm gave a wall-storage lifetime τ_{wall} of 76 s. Hence, for the optimization, we assumed a range of 60 s to 100 s for τ_{wall} . Reaching the required isotopic purity for dozens of liters of helium is difficult with conventional purification methods [41]. Instead we rely on commercially available helium with a ^3He abundance of 10^{-12} [42, 43], resulting in an absorption lifetime τ_{abs} of several thousand seconds, so we assumed its contribution to be negligible. See table 2 for the range of assumptions made in the optimizations.

Table 2: Range of assumptions for parameters in the UCN-density estimator ρ .

Parameter	Range
τ_{wall}	60 s to 100 s
τ_{β}	880 s
τ_{abs}	∞
B	500 s to 1500 s
a	-1.5 to -1.0
$V_{\text{guides}} + V_{\text{EDM}}$	100 L to 200 L
Q_{static}	0 W to 1 W

4. Optimization

4.1. Optimization goal

The primary goal of the TUCAN collaboration is to do a measurement of the neutron electric dipole moment (nEDM) with a sensitivity of $10^{-27} e \text{ cm}$. This requires a large number of UCN in the storage cell of the experiment and the source should be designed in such a way that it maximizes the number of UCN that can be delivered to the cell. How many of the produced UCN can actually reach the experiment is largely dominated by losses in the UCN guides between source and experiment, but these losses are not affected by changes in the geometry of the source. If we assume the guide losses are fixed, the source itself has only three parameters that affect the density delivered to the experiment:

- UCN-production rate P ,
- storage lifetime of UCN in the source τ , and
- volume of the source V_{source} .

To optimize only the source itself, we can use an estimator for the UCN density in the cell ρ , given by the total number of UCN produced in the source $P\tau$ diluted into the volume of the whole system $V = V_{\text{source}} + V_{\text{guides}} + V_{\text{nEDM}}$:

$$\rho = \frac{P\tau}{V}. \quad (10)$$

Assuming the UCN guides in the source are 3.0 m long and have a diameter of 150 mm, and the guides to the experiments are 9.5 m long and have a diameter of 95 mm, we get $V_{\text{guides}} = 120 \text{ L}$. The two nEDM cells will have a volume of about 30 L each, totaling $V_{\text{guides}} + V_{\text{EDM}} \approx 180 \text{ L}$. To account for potential changes of guide diameters and storage experiments with different volumes, we assumed a range between 100 L and 200 L, see table 2.

During the initial parameter studies we kept the dimensions of the UCN-converter volume constant. Since in that case the factor V in the density estimator $\frac{P\tau}{V}$ is constant and the storage lifetime τ depends only on heat load Q , we can instead optimize the production-to-heat ratio P/Q .

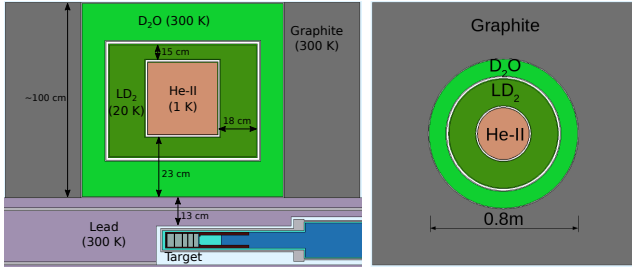


Figure 7: Cross sections of the initial moderator geometry viewed from the side (left) and top (right) with the ideal layer thicknesses indicated.

4.2. Initial parameter studies

For an initial optimization we chose well-known neutron moderators in a geometry that we assumed makes best use of the symmetry of the problem: concentric, vertical cylinders, centered above the target and filled with heavy water at room temperature, liquid deuterium at 20 K (LD_2), and superfluid helium (He-II), see Fig. 7. Graphite surrounds the whole assembly at the sides and acts as a neutron reflector. The target is encased in lead, which is relatively transparent to fast neutrons and shields much of the gamma radiation from the target.

By individually varying the thickness of bottom, radial, and top layers of thermal and cold moderator and the thickness of the lead layer above the target we were able to determine the optimal thickness for each.

The results showed that the radial liquid-deuterium layer is the most important one, achieving best performance at a thickness of 18 cm, see Fig. 7. However, safety regulations require us to minimize the amount of flammable deuterium needed. The optimization showed that this can be achieved without sacrificing performance by partly replacing the bottom deuterium layer with more heavy water—as long as the combined thickness is 23 cm or more—and reducing the thickness of the top deuterium layer to 15 cm.

The radial and upper heavy-water and graphite layers have less impact. Removing either barely changes the production-to-heat ratio, but larger thicknesses increase production and heat load proportionally, helping to scale to higher heat loads if necessary.

The lead layer between target and moderators should ideally be 13 cm thick, however this can be reduced to again achieve higher production and heat loads while only slightly reducing their ratio.

4.3. Specific parameter studies

4.3.1. Converter-vessel materials

Since roughly 50% of the heat load on the UCN converter is deposited in the vessel walls (see Fig. 3) we investigated a range of materials to try to reduce that, see table 3. The ideal material to use is beryllium, thanks to its high strength, low density, low gamma absorption, and low neutron absorption. However, it is extremely expensive.

Table 3: Effect of different materials (cf. table 1) of the superfluid-helium vessel on the production-to-heat ratio, relative to pure aluminium. The wall thickness is roughly scaled with the yield strength of each material.

Material	Thickness (mm)	Effect on P/Q (%)
Aluminium	2	(baseline)
Al6061	2	-5
AlBeCast 910	3	+5
AlBeMet 162	2	+50
AZ80	2.5	+40
BerAlCast 310	1.5	-5
Beryllium	1.5	+90
Magnox AL80	4	+15

Other promising materials are magnesium-aluminium alloys like AZ80 and beryllium-aluminium alloys like AlBeMet. Constituents to avoid are e.g. manganese and silver. These have high neutron absorption and can bring down the performance, e.g. in the case of BerAlCast. However, compared to these more exotic materials, aluminium 6061 has much better known strength and radiation resistance, so we chose it as the default material. We are currently considering AlBeMet as a potential future upgrade.

4.3.2. Effect of deuterium temperature and contaminations

The deuterium-liquefaction system will operate at a pressure of 117 kPa, giving melting and boiling points of 19 K and 24 K [44]. In this temperature range the deuterium density varies from 0.18 g cm^{-3} to 0.16 g cm^{-3} with the former giving a 5% higher production-to-heat ratio.

Deuterium comes in two spin states, para- and ortho-deuterium. Ortho-deuterium offers better neutron moderation. In thermal equilibrium the fraction of para-deuterium is between 2% at 20 K and 33% at room temperature [45]. To determine its effect on the performance of the source, we replaced the ortho-deuterium used for the optimization so far with 100% para-deuterium. This caused a drop in production-to-heat ratio by 20%. Since the actual fraction of para-deuterium is at least three times lower, we expect an at least three times smaller reduction of the production-to-heat ratio.

Para-ortho converters are available to reduce the fraction of para-deuterium in the supplied deuterium gas while it is liquefied. Due to the expected small effect on performance, we currently consider adding a para-ortho converter to the gas handling system a low priority and a future upgrade.

Hydrogen contamination in the deuterium gas, however, is a bigger issue. Each percent of hydrogen contamination would cause a 4% reduction in the production-to-heat ratio. Isotopic purity of commercially available deuterium is typically quoted as 99.8% [46].

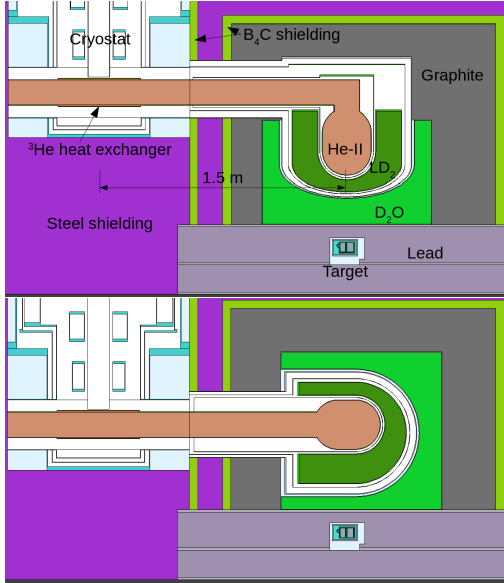


Figure 8: Cross section of more realistic simulation models with two different options to extract UCN from the converter through a UCN guide. *Top*: vertical extraction. *Bottom*: horizontal extraction. The distance between converter and heat exchanger was later increased to 2.5 m to better shield the cryostat from radiation.

Table 4: Effect of different cold moderators on the production-to-heat ratio in individually optimized geometries.

Moderator	Average layer thickness (cm)	Volume (L)	Effect on P/Q (%)
Ortho-LD ₂	12.5	125	+160
Ortho-LD ₂	19.4	200	+230
Solid D ₂ O	11.6	95	(baseline)
Para-LH ₂	3.6	33	-15

4.3.3. UCN extraction

Based on the ideal moderator thicknesses determined in the initial parameter studies, we implemented more detailed geometries, including realistic shapes of the pressure vessels, realistic vessel thicknesses, an additional explosion-proof wall between the deuterium and UCN-converter vessel, UCN guides connecting the converter to a cryostat, a ^4He - ^3He heat exchanger, and shielding materials, see Fig. 8.

The production-to-heat ratio differed by less than 1% between the two options, so we chose the horizontal extraction as it is the mechanically more feasible.

4.3.4. Other cold moderators

The large quantities of liquid deuterium required for the cold moderator pose a substantial safety risk. Therefore we also considered other cold moderators: solid heavy water, liquid hydrogen, solid methane, and mesitylene.

Solid heavy water has the advantage of being inert and easy to handle. However, measurements of its neutron-moderation properties showed that it cannot moderate

neutrons below an effective neutron temperature of about 80 K [47], reducing the neutron flux at energies where they can be converted to UCN. The exact scattering properties of solid heavy water are also not very well known—MCNP does not contain a dedicated scattering kernel as it does for liquid (heavy) water, graphite, deuterium, and hydrogen [32]. Instead, we had to use a free-gas model at an effective temperature of 80 K, adding doubts about the validity of the results.

Liquid hydrogen has a larger neutron-scattering cross section, reducing the required layer thickness. Although as flammable as deuterium, it would require less volume and reduce safety challenges. However, hydrogen has a 600 times higher neutron-absorption cross section, drastically reducing the time neutrons spend in the cold moderator and converter, reducing UCN production. The increased absorption rate also increases the heat load on the UCN converter due to the gamma radiation generated during the absorption process.

Solid methane and mesitylene could provide significantly higher cold-neutron flux, but they also rely on their large abundances of hydrogen to moderate neutrons, leading to the same issues as with liquid hydrogen. Deuterated variants could avoid that, however no good neutron-moderation data is available for those. Solid moderators are also prone to sudden releases of accumulated Wigner energy, which can lead to a catastrophic failure of their vessel. Due to these reasons we did not study them further.

Using a multi-parameter optimization, similar to the one described in section 4.4 but with a constant converter volume, we were able to find the ideal layer thicknesses for each moderator and do a fair comparison of their performance in the UCN source, see table 4. Since safety regulations limit the volume of liquid deuterium to 150 L, we ran the optimization for different volumes of liquid deuterium to estimate how a safety-related limit impacts the performance.

The results show that liquid deuterium can offer 2.6 to 3.3 times higher performance than solid heavy water, and 3.0 to 3.9 times higher performance than liquid hydrogen.

4.3.5. Bismuth neutron filter

Bismuth has a low neutron-absorption cross section and, thanks to its high density, is a good gamma shield. Especially polycrystalline bismuth is often used as a cold-neutron filter since its neutron-scattering cross section sharply drops by at least an order of magnitude for neutrons below an energy of 2 meV [48, 49], just above the energy range where the UCN-production cross section peaks.

We tried to make use of these properties with a 5 cm-thick layer of polycrystalline bismuth between the cold moderator and the UCN converter. Ideally, the bismuth would block gamma radiation and thermal neutrons and be almost transparent for cold neutrons, reducing the heat load on the UCN converter.

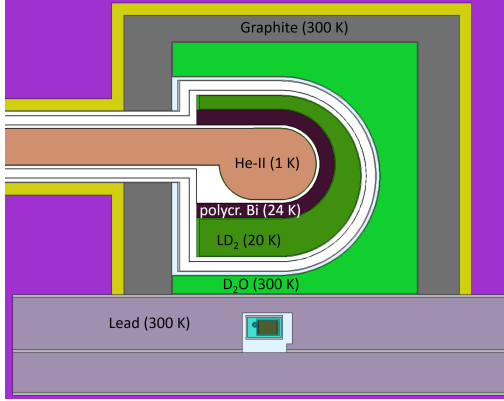


Figure 9: Moderator geometry with 5 cm-thick layer of polycrystalline bismuth.

The simulation showed that such a bismuth layer indeed reduced the heat load to the converter and its vessel by 46%. However, the added material and the reduction in LD₂-layer thickness to keep its volume below the safety limit also reduced UCN production by 36%, resulting in an increase in production-to-heat ratio of 27% compared to a configuration without bismuth. Additionally, the bismuth—being coupled to the cold moderator at 20 K—increased the heat load on the cold moderator by almost 200% and increased residual radioactivity after long-term operation ten-fold.

4.4. Full optimization

Before further optimizing the moderator geometry, we estimated the wall thicknesses required to withstand all overpressure scenarios (e.g. 3 mm for the converter vessel) and connected the UCN guide to the top of the UCN-converter to minimize the diameter of the penetration through the shielding. And we closed the heavy-water and deuterium vessels around the helium vessel, giving an improvement in estimated UCN density of 15%.

Then we implemented a multi-parameter optimization, varying eight parameters (see red labels in Fig. 10) simultaneously:

- (1) thickness of lead above target,
- (2) thickness of heavy-water layer above target,
- (3) horizontal offset between UCN-converter volume and liquid-deuterium vessel (=0 cm in Fig. 10, not shown),
- (4) length of the liquid-deuterium vessel,
- (5) horizontal offset between target and UCN-converter vessel,
- (6) radius of the UCN-converter vessel,
- (7) length of the UCN-converter vessel, and
- (8) vertical offset between liquid-deuterium vessel and UCN-converter vessel,

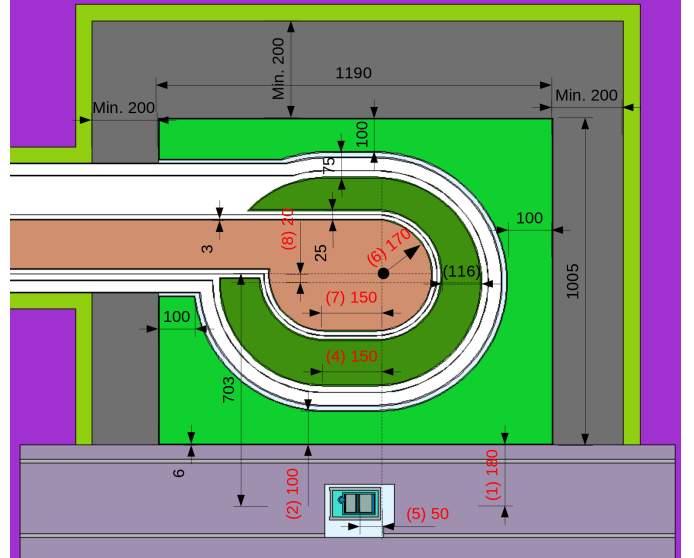


Figure 10: Dimensions (all in mm) of an average reference geometry determined from full optimizations with a range of model assumptions. Optimized parameters are indicated in red font. The thickness of the cold moderator (in parentheses) is chosen such that its total volume is 125 L. Vessel walls have a thickness of 3.6 mm, unless otherwise indicated.

while adjusting the radius of the liquid-deuterium vessel to keep its volume fixed. After each parameter change the optimization program performs the MCNP simulation and tries to find the set of parameters that maximizes the density estimator $\rho = P\tau/V$ (equation 10).

To keep the total liquid-deuterium inventory below the safety limit of 150 L, we fixed the cold-moderator volume to 125 L—taking into account up to 25 L of additional liquid in piping and heat exchangers. We performed the optimization for different combinations of assumptions for the parameters in table 2. From this set of optimized geometries we chose an “average” geometry (see Fig. 10). This average geometry turned out to be very robust—its performance differed by less than 2% from the set of optimized geometries.

4.5. Methodology

We modeled the simulation geometries in Flair [50], a GUI for the particle-transport simulation Fluka [51], and then exported them to MCNP [31]. The optimization parameters were adjusted by a custom Python program and then optimized using the SLSQP algorithm from the SciPy.optimize library [52]. The MCNP simulations were performed on Compute Canada computing clusters. Git and GitHub proved to be valuable tools to manage the large number of simulation models accumulated during the optimization.

4.6. Most important parameters

The performance of the source is rather robust against changes of the vessel sizes. Multiple iterations of the optimization resulted in differences of a few centimeters, but

Table 5: Possible improvements of the moderator geometry ranked by their potential performance increase.

Improvement	Increase in UCN density
Beryllium converter vessel	90 %
AlBeMet or AZ80 converter vessel	30 % to 50 %
Thinner converter vessel	25 % per mm
Increased LD ₂ volume	5 % per 15 L
Thinner vacuum separator/LD ₂ vessel	5 % per mm
Thinner thermal shield/D ₂ O vessel	2.5 % per mm
Reduced spacing around converter	0.5 % per mm

the estimated density varied by less than 2%. The exception is the cold moderator. Adding 15 L of liquid deuterium increases UCN production by 23 % and heat load by 14 %. See table 5 for the resulting effect on estimated UCN density.

Much more critical are thicknesses of vessel walls. Especially the UCN-converter vessel directly contributes to the heat load, making up about 50 % of the total heat load on the converter. Reducing its thickness or changing its material has the largest impact on the performance of the source, e.g. a converter vessel made of AlBeMet can increase UCN production by 18 % and reduce heat load by 25 %. AZ80 magnesium alloy can increase UCN production by 9 % and reduce heat load by 33 %. The effect on UCN density in the EDM cell depends on the assumptions, see the estimated range of improvement in table 5.

The other vessel walls also absorb neutrons, reducing UCN-production rate. This effect is most important for the walls between the cold moderator and converter, where an increase of 1 mm in thickness of any of those walls causes a drop in UCN production by 5 %. The walls between the thermal and cold moderators have about half as much impact since they are in a region with higher-energy neutrons.

The spacing between the converter vessel and the cold-moderator vessel also has slight impact on UCN production. Increasing the spacing by 10 mm reduces UCN production by 5 %.

5. Result

The fully optimized geometry shown in Fig. 10 served as a basis for detailed engineering of the pressure vessels. Detailed stress simulations with ANSYS to minimize the wall thicknesses showed that the liquid-deuterium vessel would have to have thicker walls to withstand a potential hydrogen explosion, while the converter vessel could be thinned. Especially the welds connecting the hemispherical and straight sections weaken the temper of the aluminium alloy, requiring a locally thicker wall. All changes in vessel sizes, wall thicknesses, and materials were implemented in the simulation to check their impact on performance, and the geometry was re-optimized if necessary.

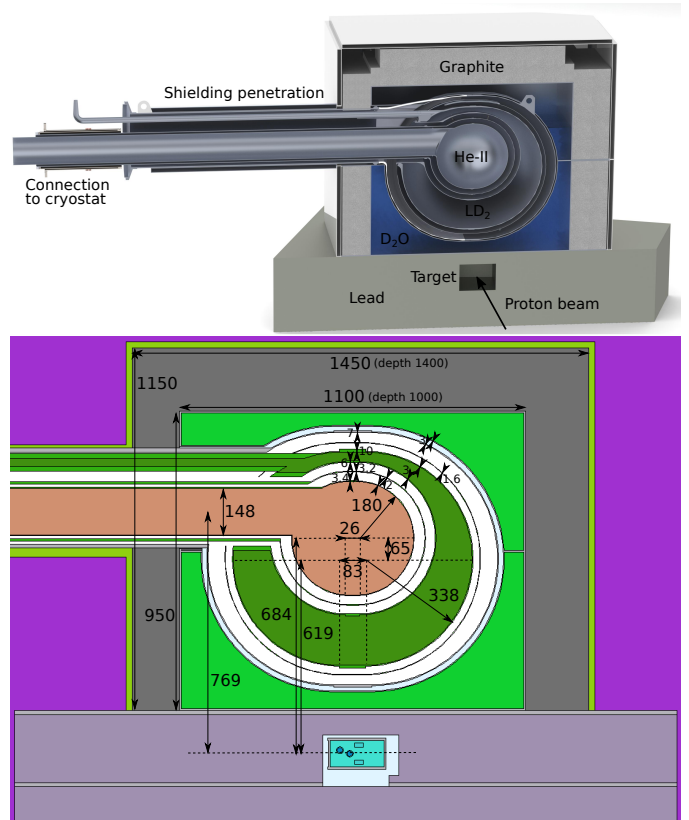


Figure 11: Detailed concept for the moderator vessels and reflectors (top) and the corresponding simulation model (bottom). The proton beam points into the page.

Table 6: Volumes, maximum heat loads, and heat loads averaged over a duty cycle of 25% with the detailed engineering model. The UCN-converter volume does not include the conduction channel.

	Volume (L)	Heat load (W)	
		max.	average
UCN converter	27	8.1	2.8
Liquid deuterium	125	63	21
Heavy water	630	430	150

With these engineering restrictions, the optimization favored a stronger aluminium 2219 alloy and almost spherical vessel shapes, since they allow to connect the two hemispherical shells with a single weld, see Fig. 11.

We also used a similar optimization to minimize the volume and therefore cost of the heavy-water and graphite reflectors, while keeping the drop in performance to less than 5%. The minimum amounts required were 630 L of heavy water and at least 15 cm of graphite on all sides of the heavy-water vessel.

UCN production and heat load are maximized if the vessels are placed right above the target. However, UCN density is maximized if they are moved upstream and left of the proton beam (out of the page and left in Fig. 11), most likely due to the asymmetry introduced by the UCN guide. The optimal offset can reach 50 cm, depending on the assumptions (cf. table 2), but the shielding arrangement allows only small offsets of about 10 cm.

With this more detailed geometry we expect UCN production of $1.6 \cdot 10^7 \text{ s}^{-1}$ and heat loads as shown in table 6. As expected, the largest fluxes of thermal and cold neutrons are found in the thermal and cold moderators (Fig. 12). The neutron spectrum in the converter has its maximum slightly above 1 meV due to only partial thermalization in the cold moderator.

[?] suggests that using the standard ^4He -scattering kernel in MCNP overestimates UCN production, since superfluid ^4He is a less efficient neutron moderator. Following their approach of reducing the ^4He density by 90% to take this into account reduces UCN production by 13% to $1.4 \cdot 10^7 \text{ s}^{-1}$. Tritium production was also estimated at about 200 GBq per year when operating at 25% duty cycle, with most of it occurring in the heavy-water and liquid-deuterium moderators.

6. Conclusions

Thanks to extensive simulations and optimization we found a geometry of neutron moderators and superfluid-helium UCN converter that performs close to optimally for a wide range of assumptions on UCN-storage lifetime in the source, cooling power of the cryostat, and attached experiments with volumes of up to 100 L. The liquid-deuterium moderator was fixed to a volume of 125 L, to stay below the safety limit of 150 L. This geometry served

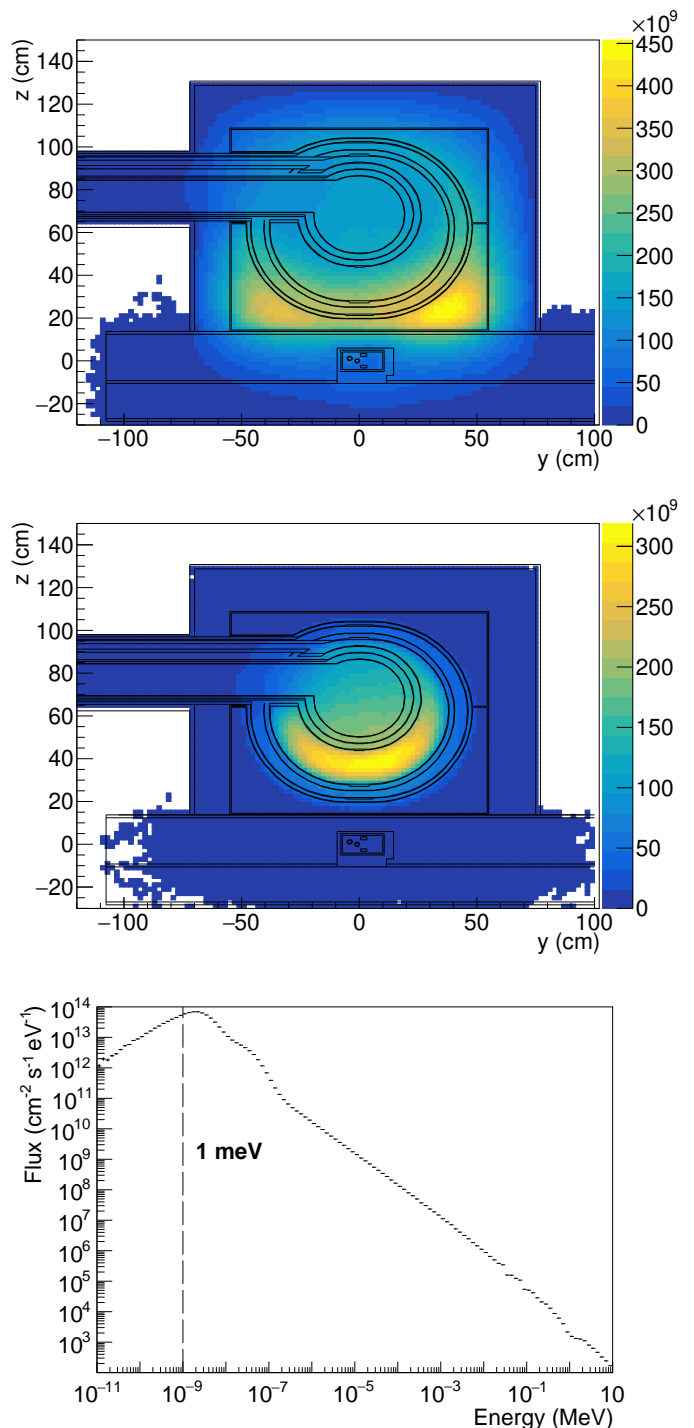


Figure 12: Neutron flux per cm^2 and s for thermal neutrons ($6 \text{ meV} < E < 100 \text{ meV}$, top) and cold neutrons ($E < 6 \text{ meV}$, middle); and the neutron spectrum in the converter (bottom).

as a baseline for detailed engineering of the pressure vessels, taking into account various safety constraints, and the simulations continued to guide all design decisions.

The final design has a converter volume of 27 L, has a liquid-deuterium volume of 125 L, and achieves a simulated UCN production of $1.4 \cdot 10^7 \text{ s}^{-1}$ to $1.6 \cdot 10^7 \text{ s}^{-1}$ at a heat load of 8.1 W. The most critical parameters are the choice of cold moderator and material of the converter vessel. With a liquid-deuterium moderator the UCN density delivered to a typical UCN-storage experiment is about three times higher than with solid heavy water or liquid hydrogen. AlBeMet, a beryllium-aluminium alloy, is a promising material for the converter vessel and could improve the performance by 30% to 50% compared to aluminium 6061.

The new moderator vessels and source are scheduled to be installed above the spallation target beginning of 2021, with commissioning starting the same year. The projected performance will enable the TUCAN collaboration to measure the neutron electric dipole moment with a sensitivity of 10^{-27} e cm .

7. Acknowledgments

We would like to thank P. Carlson and M. Chin for their early contributions to this work and Y.-S. Cho for providing an MCNP scattering kernel for polycrystalline bismuth.

This work was supported by the Canada Fund for Innovation (CFI), the Natural Sciences and Engineering Research Council of Canada (NSERC), and Compute Canada.

8. References

References

- [1] Y. B. Zel'dovich, Storage of cold neutrons, *JETP* 9 (1959) 1389.
- [2] V. I. Lushchikov, Y. N. Pokotilovskii, A. V. Strelkov, F. L. Shapiro, Observation of ultracold neutrons, *JETP Letters* 9 (1969) 23.
- [3] A. Steyerl, Measurements of total cross sections for very slow neutrons with velocities from 100 m/sec to 5 m/sec, *Physics Letters B* 29 (1) (1969) 33 – 35. doi:10.1016/0370-2693(69)90127-0.
- [4] L. Groshev, et al., Experiments with ultracold neutrons, *Physics Letters B* 34 (4) (1971) 293 – 295. doi:10.1016/0370-2693(71)90608-3.
- [5] J. Robson, D. Winfield, The detection of ultra-cold neutrons by the activation of manganese, *Physics Letters B* 40 (5) (1972) 537 – 538. doi:10.1016/0370-2693(72)90475-3.
- [6] I. Altarev, et al., A liquid hydrogen source of ultra-cold neutrons, *Physics Letters A* 80 (5) (1980) 413 – 416. doi:10.1016/0375-9601(80)90784-7.
- [7] A. Steyerl, A neutron turbine as an efficient source of ultracold neutrons, *Nuclear Instruments and Methods* 125 (3) (1975) 461 – 469. doi:10.1016/0029-554X(75)90265-7.
- [8] A. Steyerl, et al., A new source of cold and ultracold neutrons, *Phys. Lett. A* 116 (7) (1986) 347 – 352. doi:10.1016/0375-9601(86)90587-6.
- [9] R. Golub, J. Pendlebury, Super-thermal sources of ultra-cold neutrons, *Phys. Lett. A* 53 (2) (1975) 133 – 135. doi:10.1016/0375-9601(75)90500-9.
- [10] R. Golub, K. Böning, New type of low temperature source of Ultra-cold neutrons and production of continuous beams of UCN, *Zeitschrift für Physik B Condensed Matter* 51 (2) (1983) 95–98. doi:10.1007/BF01308763.
- [11] A. Saunders, et al., Demonstration of a solid deuterium source of ultra-cold neutrons, *Physics Letters B* 593 (1) (2004) 55 – 60. doi:10.1016/j.physletb.2004.04.048.
- [12] A. Frei, et al., First production of ultracold neutrons with a solid deuterium source at the pulsed reactor triga mainz, *The European Physical Journal A* 34 (2) (2007) 119–127. doi:10.1140/epja/i2007-10494-2.
- [13] A. Anghel, et al., The PSI ultra-cold neutron source, *Nucl. Instrum. Methods Phys. Res. A* 611 (2) (2009) 272 – 275, particle Physics with Slow Neutrons. doi:10.1016/j.nima.2009.07.077.
- [14] S. A. Wlokka, Aspects of Ultra-Cold Neutron Production in Radiation Fields at the FRM II, Dissertation, Technische Universität München, München (2016).
- [15] E. Korobkina, et al., Ultracold neutron source at the PULSTAR reactor: Engineering design and cryogenic testing, *Nucl. Instrum. Methods Phys. Res. A* 767 (2014) 169 – 175. doi:10.1016/j.nima.2014.08.016.
- [16] H. Yoshiaki, K. Sakai, T. Kawai, S. Goto'o, Three metre long horizontal cryostat producing ultracold neutrons using superfluid liquid helium at 0.5 K (Mark 3000), *Cryogenics* 34 (4) (1994) 277 – 286. doi:10.1016/0011-2275(94)90107-4.
- [17] F. M. Piegsa, et al., New source for ultracold neutrons at the Institut Laue-Langevin, *Phys. Rev. C* 90 (2014) 015501. doi:10.1103/PhysRevC.90.015501.
- [18] E. P. Tsentalovich, nEDM Collaboration, The nedm experiment at the sns, *Physics of Particles and Nuclei* 45 (1) (2014) 249–250. doi:10.1134/S1063779614011073.
- [19] C. OShaughnessy, et al., Measuring the neutron lifetime using magnetically trapped neutrons, *Nucl. Instrum. Methods Phys. Res. A* 611 (2) (2009) 171 – 175, particle Physics with Slow Neutrons. doi:10.1016/j.nima.2009.07.054.
- [20] E. Lychagin, et al., UCN sources at external beams of thermal neutrons. An example of PIK reactor, *Nucl. Instrum. Methods Phys. Res. A* 823 (2016) 47 – 55. doi:10.1016/j.nima.2016.04.008.
- [21] Y. Masuda, et al., Spallation Ultracold Neutron Source of Superfluid Helium below 1 K, *Phys. Rev. Lett.* 108 (2012) 134801. doi:10.1103/PhysRevLett.108.134801.
- [22] S. Ahmed, et al., First ultracold neutrons produced at TRIUMF, *Phys. Rev. C* 99 (2019) 025503. doi:10.1103/PhysRevC.99.025503.
- [23] S. Ahmed, et al., A beamline for fundamental neutron physics at TRIUMF, *Nucl. Instrum. Methods Phys. Res. A* 927 (2019) 101 – 108. doi:10.1016/j.nima.2019.01.074.
- [24] S. Ahmed, et al., Fast-switching magnet serving a spallation-driven ultracold neutron source, *Phys. Rev. Accel. Beams* 22 (2019) 102401. doi:10.1103/PhysRevAccelBeams.22.102401.
- [25] A. Serebrov, et al., Supersource of ultracold neutrons at WWRM reactor in PNPI and the research program on fundamental physics, *Physics Procedia* 17 (2011) 251 – 258, 2nd International Workshop on the Physics of fundamental Symmetries and Interactions - PSI2010. doi:10.1016/j.phpro.2011.06.044.
- [26] K. K. H. Leung, et al., A next-generation inverse-geometry spallation-driven ultracold neutron source, *Journal of Applied Physics* 126 (22) (2019) 224901. doi:10.1063/1.5109879.
- [27] P. Schmidt-Wellenburg, et al., Experimental study of ultracold neutron production in pressurized superfluid helium, *Phys. Rev. C* 92 (2015) 024004. doi:10.1103/PhysRevC.92.024004.
- [28] E. Korobkina, R. Golub, B. Wehring, A. Young, Production of UCN by downscattering in superfluid He4, *Physics Letters A* 301 (5) (2002) 462 – 469. doi:10.1016/S0375-9601(02)01052-6.
- [29] K. K. H. Leung, S. Ivanov, F. M. Piegsa, M. Simson, O. Zimmer, Ultracold-neutron production and up-scattering in superfluid helium between 1.1 K and 2.4 K, *Phys. Rev. C* 93 (2016) 025501. doi:10.1103/PhysRevC.93.025501.

- [30] M. Tanabashi, et al., Review of particle physics, Phys. Rev. D 98 (2018 and 2019 update) 030001. doi:10.1103/PhysRevD.98.030001.
- [31] T. Goorley, et al., Initial MCNP6 Release Overview, Nuclear Technology 180 (3) (2012) 298–315. doi:10.13182/NT11-135.
- [32] M. Chadwick, et al., ENDF/B-VII.0: Next Generation Evaluated Nuclear Data Library for Nuclear Science and Technology, Nuclear Data Sheets 107 (12) (2006) 2931 – 3060, evaluated Nuclear Data File ENDF/B-VII.0. doi:10.1016/j.nds.2006.11.001.
- [33] Sherritt Technologies, Analytical Laboratory Services (2016). URL <https://www.sherritt.com/English/operations/Commercial-and-Technologies/Capabilities/Analytical-Laboratory-Services-/default.aspx>
- [34] Toyo Tanso, Special Graphite Property Data (2018). URL https://www.toyotanso.com/Products/Special_graphite/data.html
- [35] Materion Corporation, AlBeCast Composite Design Guide (2019). URL <https://materion.com/products/metal-matrix-composites/albecast-investment-casting-alloys>
- [36] Materion Corporation, AlBeMet Technical Fact Sheet (2019). URL <https://materion.com/products/metal-matrix-composites/albemet>
- [37] IBC Advanced Alloys, Product Data Sheet - Beralcast 310 (2019). URL <https://ibcadvancedalloys.com/home/products/beryllium-products/beralcast/>
- [38] S. W. Van Sciver, Helium cryogenics, Springer Science & Business Media, 2012.
- [39] Cryodata.Inc., HEPAK User’s Guide, Horizon Technologies, 2005. URL <http://www.htess.com/hepak.htm>
- [40] C. J. Gorter, J. H. Mellink, On the irreversible processes in liquid helium II, Physica 15 (3) (1949) 285 – 304. doi:10.1016/0031-8914(49)90105-6.
- [41] P. McClintock, An apparatus for preparing isotopically pure He4, Cryogenics 18 (4) (1978) 201 – 208. doi:10.1016/0011-2275(78)90002-4.
- [42] P. Hendry, P. McClintock, Continuous flow apparatus for preparing isotopically pure 4He, Cryogenics 27 (3) (1987) 131 – 138. doi:10.1016/0011-2275(87)90069-5.
- [43] H. P. Mumm, et al., High-sensitivity measurement of ^3He – ^4He isotopic ratios for ultracold neutron experiments, Phys. Rev. C 93 (2016) 065502. doi:10.1103/PhysRevC.93.065502.
- [44] S. Ahmed, et al., Conceptual Design Report for the Next Generation UCN Source at TRIUMF (2018).
- [45] K. Mishima, Irradiation effect of Ortho deuterium for UCN source, Ph.D. thesis, Osaka University (2004).
- [46] Praxair, Compressed Deuterium Gas Spec Sheet (2019). URL <https://www.praxair.com/gases/buy-deuterium-gas>
- [47] J. J. Rush, D. W. Connor, R. S. Carter, Study of D2O Ice as a Cold-Neutron Source, Nuclear Science and Engineering 25 (4) (1966) 383–389. doi:10.13182/NSE66-A18558.
- [48] M. Adib, M. Kilany, On the use of bismuth as a neutron filter, Radiation Physics and Chemistry 66 (2) (2003) 81 – 88. doi:10.1016/S0969-806X(02)00368-7.
- [49] Y.-S. Cho, J. Chang, The calculation of neutron scattering cross sections for silicon and bismuth crystal at thermal energies, Journal of Nuclear Science and Technology 39 (sup2) (2002) 176–179. doi:10.1080/00223131.2002.10875069.
- [50] V. Vlachoudis, et al., FLAIR: a powerful but user friendly graphical interface for FLUKA, in: Proc. Int. Conf. on Mathematics, Computational Methods & Reactor Physics (M&C 2009), Saratoga Springs, New York, Vol. 1, 2009, p. 3.
- [51] A. Ferrari, P. R. Sala, A. Fasso, J. Ranft, FLUKA: A multi-particle transport code (Program version 2005) (2005).
- [52] D. Kraft, A software package for sequential quadratic programming, Tech. Rep. DFVLR-FB 88-28, DLR German Aerospace Center Institute for Flight Mechanics, Köln, Germany (1988).